

Stability of Cauchy Horizon under perturbations

Flavio Henrique and Elcio Abdalla

Instituto de Fisica, Universidade de Sao Paulo, C.P.66.318, CEP 05315-970, Sao Paulo

(Dated: February 2004)

We use perturbations in order to study the stability of the Cauchy Horizon in a Reissner-Nordström space-time. The perturbations are either scalar or gravitational, and indicate some strong instabilities.

I. INTRODUCTION

Statistically, most of the Black Holes in the Universe should belong to the kind described by the Kerr solution, characterized by the existence of an external event horizon — r_+ — and an internal so called Cauchy horizon, which we denote by — r_- . Classically, an observer can cross both horizons, and instead of falling into the singularity, emerge into a new asymptotically flat universe, different from the starting one. The process can repeat indefinitely, leading the observer to new worlds [1].

Such an image is however not a complete description of the physics related to Black Holes with a Cauchy horizon. Indeed, a small perturbation inside the horizon can induce an instability which can possibly lead to a collapse of the geometry.

Moreover, there are further problems connected with the existence of a Cauchy horizon. The denomination *Cauchy horizon* is related to the fact that depending on how one crosses the surface $r = r_-$ one is outside the domain of causal dependence on the past. This means that the Cauchy horizon is the causal dependence limit $H^+(\Sigma)$ of all time-like curves that intersect a space-like surface Σ and cross the Cauchy horizon, see figure (1). In other words, the future beyond the Cauchy horizon cannot be determined exclusively from the past. In particular, for the Kerr Black Hole the region beyond the internal horizon can contain curves which are closed in time, see [2]. These curves introduce an infinite set of possible histories for any event into “causal” influence domain of “time machines”.

There seem to be difficult points for interpretation beyond the Cauchy horizon, namely crossing it is *fraught with danger* using words of Chandrasekhar [1]. Indeed, the Cauchy horizon is known to be a structure of great instability under perturbations whose intensity enlarges in its neighbourhood. In this work we study the stability of Cauchy horizon under perturbations [3, 4]. Some non-perturbative results have been obtained by [7] and [12], where instability has been found.

In this work we first choose the geometry and

study its stability for a fictitious observer traveling into the horizon in a time-like curve. Later we develop a scalar and a gravitational perturbation, after which we arrive at some conclusions.

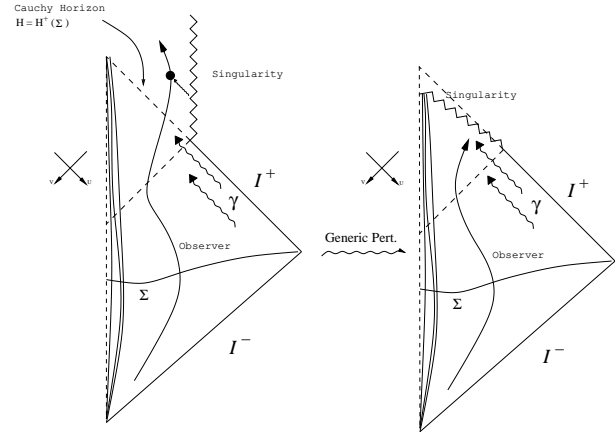


FIG. 1: Conformal diagram of the Reissner-Nordström geometry. Passing through the Cauchy horizon future gets an indetermination due to the influence of the singularity. Figure from [5].

II. GEOMETRY AND OBSERVER

It is a difficult task to work with a Kerr geometry, due to the fact that coordinates do not decouple. An easier alternative in order to study Cauchy horizons is to consider a Reissner-Nordström geometry, defined by the metric

$$ds^2 = \frac{\Delta}{r^2} dt^2 - \frac{r^2}{\Delta} dr^2 - r^2 d\theta^2 - r^2 \sin^2 \theta d\varphi^2, \quad (1)$$

where $\Delta = r^2 - 2Mr + Q^2$.

Besides representing a structure similar to the Kerr, it corresponds to the limit of the Kerr geometry for low density of angular momentum by mass, being a reasonable approximation for the problem.

We are interested in the region between the two horizons, where $\Delta < 0$. In this case the variables

r and t exchange their role (see [6]). The tortoise coordinates are, in this case, defined as

$$dt^* = -\frac{r^2}{\Delta} dr \quad , \quad dr^* = dt \quad , \quad (2)$$

where the definitions contain the new status of time and distance, respectively. Notice that $r \rightarrow r_-$ implies $t^* \rightarrow -\infty$.

We now suppose that small perturbations are generated between the two horizons, with the “energy density” measured in the reference frame of the observer as

$$\mathcal{F} = p^\mu \partial_\mu \Psi \quad , \quad (3)$$

as proposed in [3] (see also [1]). The p^μ in expression (3) corresponds to the traveller’s quadri-momentum in a free falling time-like curve into Cauchy horizon at the equator of the black hole, i. e. $\theta = \frac{\pi}{2}$ and with zero of angular momentum. Expression (3) is a part of traveller’s complete energy density which is

$$\mathcal{E} = \mathcal{F}^2 - \frac{1}{2} p^2 \partial_\mu \Psi \partial^\mu \Psi \quad ,$$

where Ψ is the perturbation. In the coordinate frame

$$u = t^* - r^* \quad , \quad v = t^* + r^* \quad (4)$$

the “energy density” is given by the expression

$$\mathcal{F} = -\frac{r^2}{(r_+ - r)(r - r_-)} \left[\left(E + \sqrt{E^2 - \frac{\Delta}{r^2}} \right) \Psi_{,v} - \left(E - \sqrt{E^2 - \frac{\Delta}{r^2}} \right) \Psi_{,u} \right] \quad , \quad (5)$$

where E is a real number between $-\infty$ and $+\infty$. Near the Cauchy horizon \mathcal{F} behaves as

$$\mathcal{F}_u \rightarrow \frac{r_-^2}{r_+ - r_-} E e^{-\frac{\kappa_-}{2} u} \Psi_{,u} \Big|_{v=v_0} \text{ for } u \rightarrow -\infty \quad ,$$

$$\mathcal{F}_v \rightarrow -\frac{r_-^2}{r_+ - r_-} E e^{-\frac{\kappa_-}{2} v} \Psi_{,v} \Big|_{u=u_0} \text{ for } v \rightarrow -\infty \quad ,$$

with $\kappa_- = \frac{r_+ - r_-}{r_-^2}$. Supposing that the asymptotic behaviour of the perturbation is $\Psi_{,u} \rightarrow e^{\alpha u}$ and $\Psi_{,v} \rightarrow e^{\alpha v}$; one concludes that for $\alpha - \frac{\kappa_-}{2} < 0$ the perturbation is unstable since near the Cauchy horizon $|\mathcal{F}| \rightarrow \infty$. Otherwise, for $\alpha - \frac{\kappa_-}{2} > 0$ the perturbation is stable. The possibility $\alpha = \frac{\kappa_-}{2}$ implies convergence of \mathcal{F} to an asymptotic and finite number, whose amplitude depends of global evolution of Ψ , in which case the plot of \mathcal{F} is necessary.

III. SCALAR FIELD

We consider the scalar wave equation

$$\frac{1}{\sqrt{-g}} \partial_\mu \sqrt{-g} \partial^\mu \Phi(r, t, \theta, \varphi) = 0 \quad , \quad (6)$$

where $g = \det[g_{\mu\nu}] = -r^2 \sin^2 \theta$, for the Reissner-Nordström metric. We assume the usual separation in terms of spherical harmonics,

$$\Phi(r, t, \theta, \varphi) = \sum_{lm} \frac{\Psi(r, t)}{r} Y_{lm}(\theta, \varphi) \quad ,$$

Obtaining the wave equation

$$\frac{\Delta}{r^2} \frac{\partial}{\partial r} \left(\frac{\Delta}{r^2} \frac{\partial}{\partial r} \Psi(r, t) \right) - \frac{\partial^2}{\partial t^2} \Psi(r, t) = \frac{\Delta}{r^3} \left(\frac{\partial}{\partial r} \frac{\Delta}{r^2} + \frac{l(l+1)}{r} \right) \Psi(r, t) \quad ,$$

which for the tortoise coordinates (2) leads to

$$\frac{\partial^2}{\partial t^{*2}} \Psi(r^*, t^*) - \frac{\partial^2}{\partial r^{*2}} \Psi(r^*, t^*) = V_l(t^*) \Psi(r^*, t^*) \quad , \quad (7)$$

with V_l given by $V_l(t^*) = \frac{\Delta}{r^4} \left[\frac{2}{r^2} (Mr - Q^2) + l(l+1) \right]$. Using the u, v coordinates, we find, as usual,

$$4 \frac{\partial^2}{\partial u \partial v} \Psi = V_l \left(\frac{u+v}{2} \right) \Psi \quad . \quad (8)$$

Such equation is discretized as shown in figure (2) and following [10, 13], whereof we use the notation.

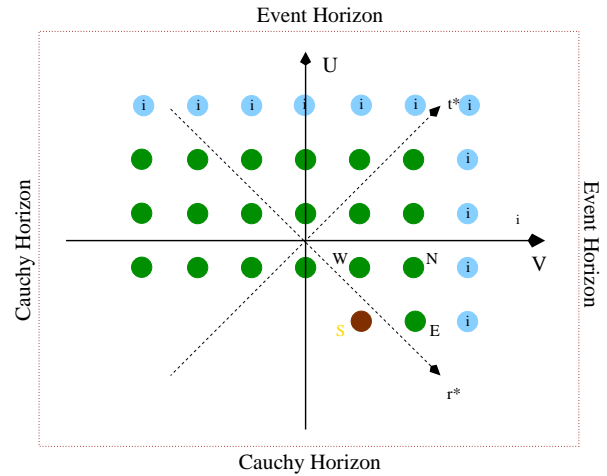


FIG. 2: Diagram corresponding to the integration grid, in the region between the two horizons, in the Reissner-Nordström metric. The cells marked with i correspond to the initial condition.

Therefore,

$$\Psi_S = (\Psi_W + \Psi_E) \left(1 + \frac{\delta v \delta u}{8} V(t_W^*) \right) - \Psi_N \quad .$$

The integration of equation (8) has been performed for all harmonics l from 0 up to 59. The results are shown in figures (3), (4) and (5). The straight line indicates the transition between stable perturbations, above the straight line, and unstable below. For l above 8 the coefficients oscillate between stability and instability, a fact observed thereafter. Further observations are here performed since enlarging the grid towards the horizons leads to the fact that all perturbations stay on the verge of stability and a more detailed investigation was required. Indeed, stable points can undergo drastic variations when one approaches the Cauchy horizon as shown in figure (5) which is analogous to figure (4), but with an enlarged grid.

On example of such a behaviour is shown in figure (6) where the function $\mathcal{F}_v|_{u_0=-240.0}$ was plotted for $l = 58$. Although from figure (5) the α coefficient indicates stability, the function \mathcal{F}_v reveals a strong increase by 16 orders of magnitude. Such a behaviour turns out to be quite general.

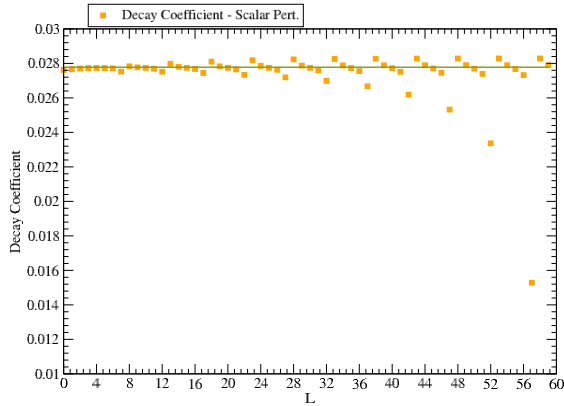


FIG. 3: α coefficients for $r_+ = 3.5$ and $r_- = 3.0$ from the asymptotic behaviour of $\Psi_{,u}|_{v_0=-300.00}$ for $r \rightarrow r_-$.

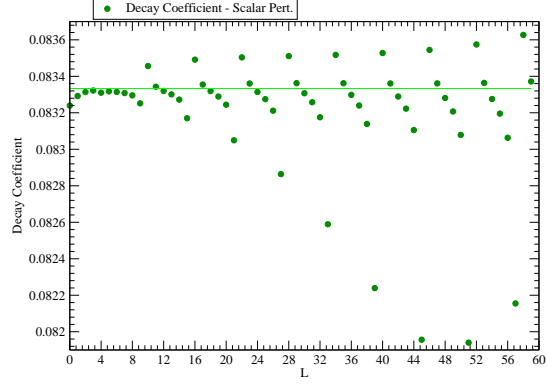


FIG. 4: α coefficients corresponding to the function $\Psi_{,v}|_{u_0=-140.00}$ for $r_+ = 4.5$ and $r_- = 3.0$. We used $\Delta u = \Delta v = 180$.

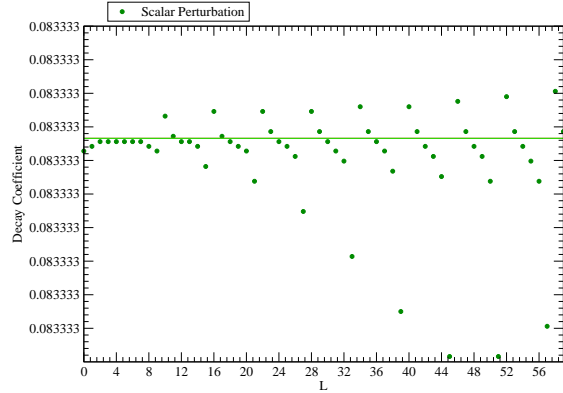


FIG. 5: α coefficients corresponding to the function $\Psi_{,v}|_{u_0=-240.00}$. Here $\Delta v = \Delta u = 280.00$. Notice that now all α 's are very near the asymptotic value $\frac{\kappa_-}{2} = 0,0833$.

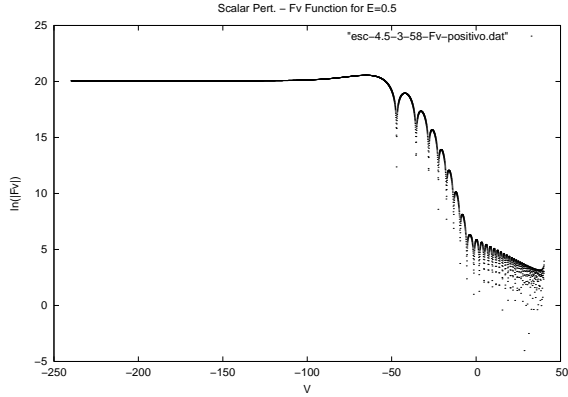


FIG. 6: Diagram showing the function $\ln|\mathcal{F}_v| \times v$ for $l = 58$. There is no sign of stability.

Furthermore, some results concerning the perturbation as function of the u , v and t^* coordinates are shown in figures (7), (8) and (9), where in those diagrams the Cauchy horizon corresponds to the far left of the diagrams. These diagrams reveal important unstabilities toward the Cauchy horizon, with an increase of three orders of magnitude in figure (7), 15 orders in figure (8), and 13 orders in figure (9), no matter what is the choice for r^* .

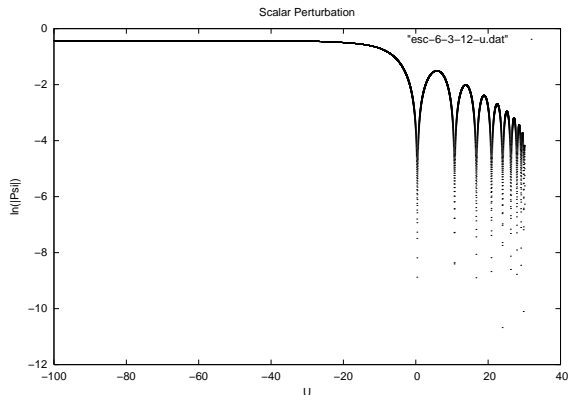


FIG. 7: Here $\ln|\Psi(u, v = -100)|$ is shown, for a scalar perturbation for $r_+ = 6.0$ and $r_- = 3.0$ with $l = 12$. Between the points (30.0) and (-100.0) there is a growth by three orders of magnitude.

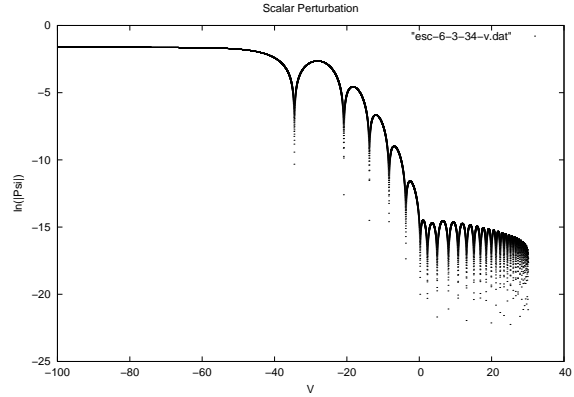


FIG. 8: Here $\ln|\Psi(u = -100, v)|$ is shown, for a scalar perturbation for $r_+ = 6.0$ and $r_- = 3.0$ with $l = 34$. There is an increase here in 15 orders of magnitude.

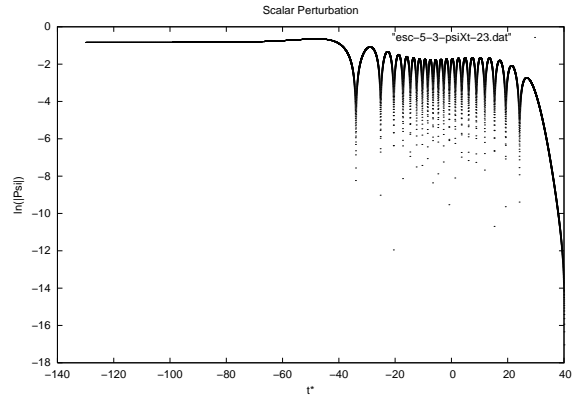


FIG. 9: Diagram of $\ln|\Psi| \times t^*$ for $r_+ = 5.0$ and $r_- = 3.0$ with $l = 23$. There is a big increase in the amplitude at the position $r^* = 0.0$ as we approach the Cauchy horizon.

Further examples have been studied with analogous results.

IV. GRAVITATIONAL PERTURBATION

We perturb the metric (1), referred to as $g_{\mu\nu}^{(0)}$, by means of a small correction $h_{\mu\nu}$ as

$$g_{\mu\nu} = g_{\mu\nu}^{(0)} + h_{\mu\nu} \quad . \quad (9)$$

We shall complement our study now about perturbations on Reissner-Nordström geometry using directly the above procedure. The perturbation (9) leads to two types of perturbations, as usual [1],

which corresponds to the scalar equation with a different potential $V_l(t^*)$, namely,

- axial:

$$V_l^-(t^*) = V_l^-(r(t^*)) = \frac{\Delta}{r^5} \left[(\mu^2 + 2)r - q + \frac{4Q^2}{r} \right],$$

- polar:

$$V_l^+(t^*) = V_l^+(r(t^*)) = V_l^- - 2q \frac{d}{dt^*} \frac{\Delta}{r^3(\mu^2 r + q)},$$

where $\mu^2 = (l-1)(l+2)$ and $q = 3M - \sqrt{9M^2 + 4Q^2\mu^2}$.

Equation (7) can again be integrated.

Figures (10) and (11) give us the results for the α 's with l from 1 up to 60

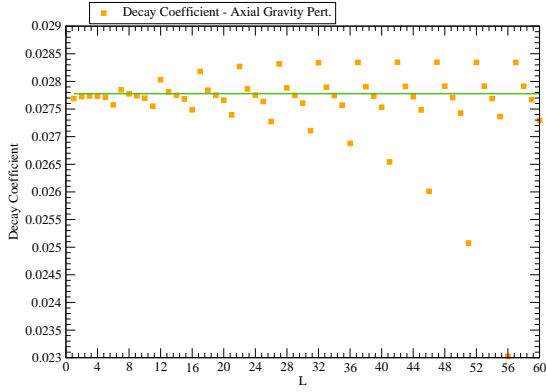


FIG. 10: α coefficients for $\Psi_{,u}|_{v_0=-300.00}$ in the asymptotic limit $r \rightarrow r_-$ for $r_+ = 3.5$ and $r_- = 3.0$.

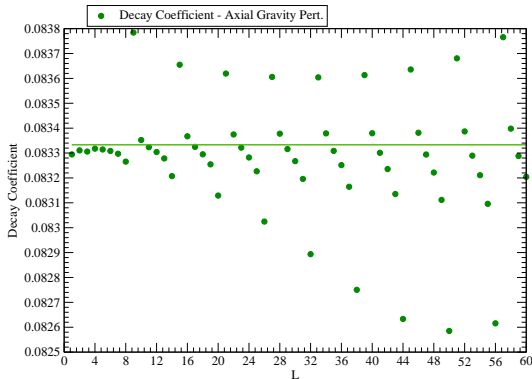


FIG. 11: α 's corresponding to $\Psi_{,v}|_{u_0=-140.00}$. Here we used $\Delta u = \Delta v = 180$.

For $l > 8$ there are again oscillations between stable and unstable points. As in the scalar field we amplify the grid of integration. Figure (12) shown results similar to those obtained for the scalar field.

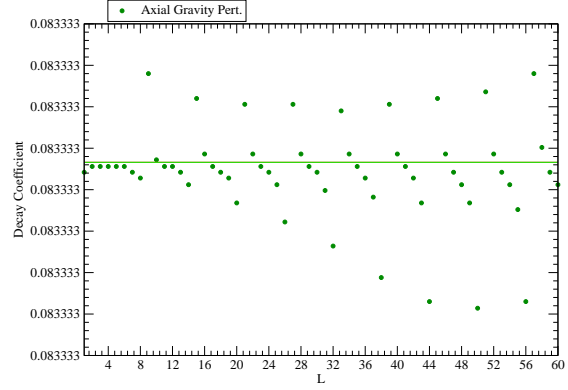


FIG. 12: α 's corresponding to $\Psi_{,v}|_{u_0=-240.00}$ using $\Delta u = \Delta v = 280.00$.

Figure (15) displays the function $\mathcal{F}_v|_{u_0=-240.00}$ for the value $l = 57$ from figure (12).

We learn again that in spite of the fact that a rough calculation of α indicated stability, in fact \mathcal{F}_v eventually undergoes an increase of 17 orders of magnitude. The same occurs with any other point in figure (12). This occurs because the α -coefficient does not stay fixed, converging to $\frac{\kappa_-}{2}$ when $v \rightarrow -\infty$.

Figures (13) and (14) shown the α coefficients for the polar perturbation for $l = 1, \dots, 21$. In contrast to the axial perturbation the coefficients

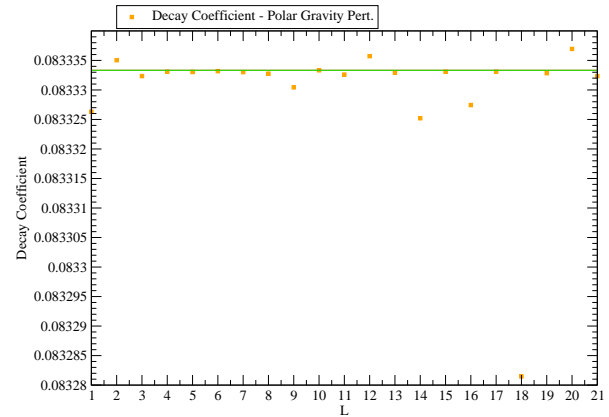


FIG. 13: α coefficients for the polar perturbation $\Psi_{,u}|_{v_0=-190.00}$ when $r_+ = 4.5$ and $r_- = 3.0$.

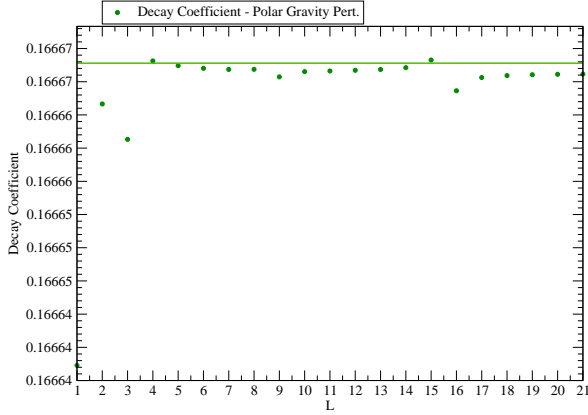


FIG. 14: α coefficients for the polar perturbation $\Psi_{,v}|_{u_0=-120.00}$ with $r_+ = 6.0$ and $r_- = 3.0$.

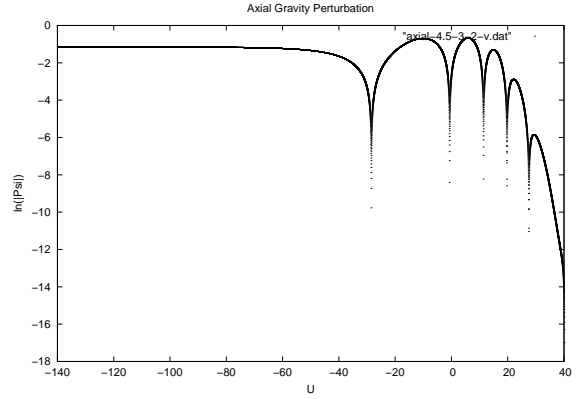


FIG. 16: $|\Psi(u = -140, v)| \times v$ for $r_+ = 4.5$ and $r_- = 3.0$ with $l = 2$.

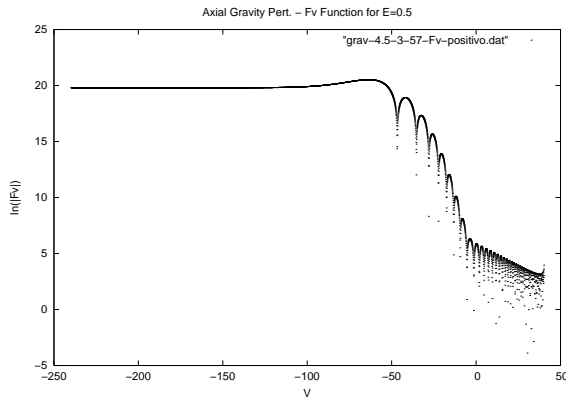


FIG. 15: $\ln|\mathcal{F}_v| \times v$ for $l = 57$. The final value of the function is 17 orders of magnitude larger than the initial value.

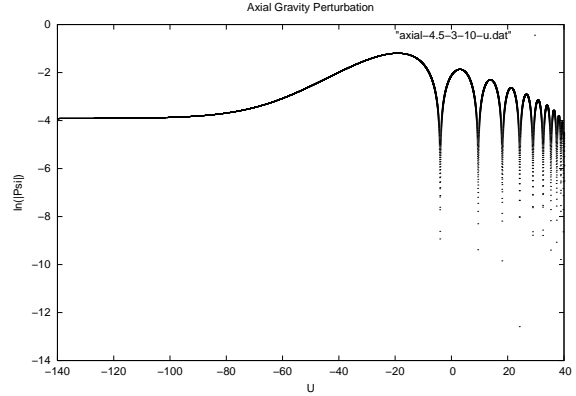


FIG. 17: $|\Psi(u, v = -140)| \times u$ for $r_+ = 4.5$ and $r_- = 3.0$ with $l = 10$.

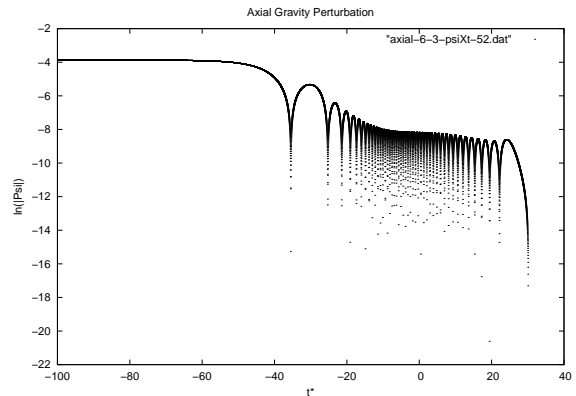
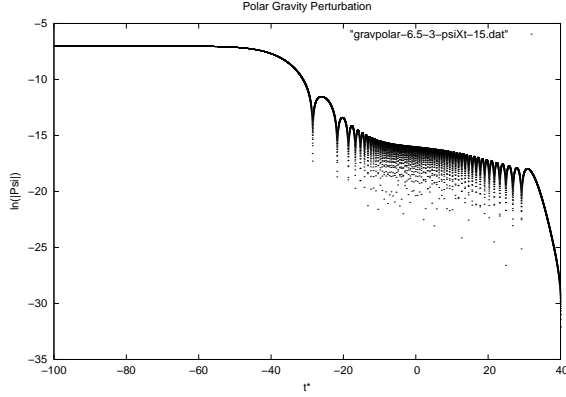
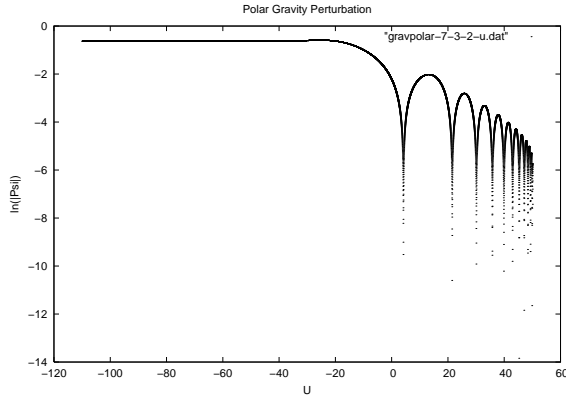
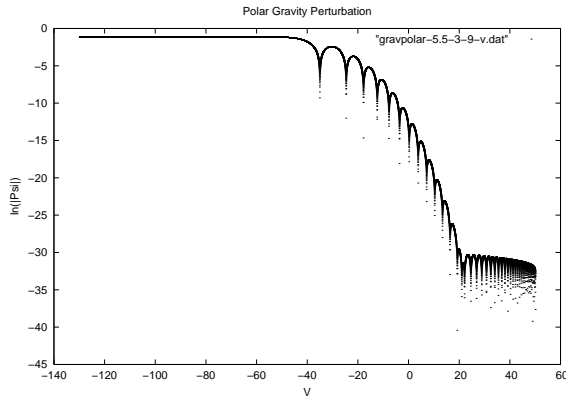


FIG. 18: $\ln|\Psi| \times t^*$ for $r_+ = 6.0$ and $r_- = 3.0$ with $l = 52$. Instability of the perturbation at $r^* = 0.0$.

We also show the perturbations of the functions V_l^\pm in figures (16), (17), (18), (19), (20) and (21). The results are similar to those obtained for scalar perturbations, with large increase of the functions toward the Cauchy horizon. Notice that polar perturbation has the most unstable results when compared with other equivalent diagrams.


 FIG. 19: $\ln|\Psi| \times t^* r_+ = 6.5$ and $r_- = 3.0$ with $l = 15$.

 FIG. 20: Polar perturbation $\ln|\Psi(u, v = -115)|$ for $r_+ = 7.0$ and $r_- = 3.0$ with $l = 2$.

 FIG. 21: Polar perturbation $\ln|\Psi(u = -130, v)|$ for $r_+ = 5.5$ and $r_- = 3.0$ with $l = 9$.

As a conclusion, polar perturbation shows even more enhanced instability.

V. CONCLUSION

The results obtained for the parameters α reveal some regions of stability. However, as we approach the Cauchy horizon these coefficients vary, eventually converging to $\frac{\kappa_-}{2}$. It is thus necessary to analyse the density of energy \mathcal{F} , as shown in figures (6) e (15), which in spite of corresponding to α parameters in the region of stability.

We also show diagrams for $\ln|\Psi| \times u$, $\ln|\Psi| \times v$ and $\ln|\Psi| \times t^*$, showing large instabilities.

The final picture is that towards the Cauchy horizon a large instability occurs, and the energy density tends to increase with no bound. It is thus possible the space-time itself gets corrected in a nonperturbative way. Thus a passage by the Cauchy horizon may be impossible, a way of preventing several possible difficulties with different Universes or problems with causality, in an example of Hawking's conjecture of chronological protection [9]. Perturbation theory of the old style fails in contrast to previous results, [8], [7] [12] and new non perturbative methods are mandatory [14].

VI. ACKNOWLEDGEMENTS

We are grateful to Dr. Carlos Molina for the assistance in the use of numerical codes. This work has been supported by FAPESP and CNPq (Brazil).

-
- [1] Chandrasekhar, S. **The Mathematical Theory of Black Holes**, Oxford University Press, 2000, ISBN 0 19 850370 9.
- [2] O'Neil, Barrett, **The Geometry of Kerr Black Holes**, A K Peters, 1995, ISBN 1-56881-019-9.
- [3] Y. Cürsel, V. D. Sandberg, I. D. Novikov and A. A. Starobinsky, **Phys. Rev. D**, **19**, 413-20, 1979.
- [4] Y. Cürsel, V. D. Sandberg, I. D. Novikov and A. A. Starobinsky, **Phys. Rev. D**, **20**, 1260-70, 1979.
- [5] Hawking, S. W. and Israel, W., **General Relativity an Einstein centenary survey**, Cambridge, 1979, ISBN 0 521 22285 0.
- [6] Hawking, S. W. and Ellis, G. F. R., **The large scale structure of space-time**, Cambridge, 1973.
- [7] Gnedin, Marianna L. and Gnedin, Nickolay Y., **Class. Quantum Grav.**, **10**, 1083-1102, 1993.
- [8] Ori, A., **Phys. Rev. Letters**, **67**, **7**, 789, 1991; Ori, A. and Flanagan, E., **Phys. Rev. D**, **53**, **4**, 1754, 1996..
- [9] Hawking, S. W., **Phys. Rev. D**, **46**, **2**, 603, 1992.
- [10] Patrick R. Brady, Chris M. Chambers, William G. Laarakkers, Eric Poisson, **Phys. Rev. D**: **064003**, 1999; Patrick R. Brady, Chris M. Chambers, William Krivan, Pablo Laguna, **Phys. Rev. D**: **7538-7545**, 1997.
- [11] C. Molina, D. Giugno, E. Abdalla and A.Saa gr-qc/0309079; Jiong-Ming Zhu, Bin Wang, Elcio Abdalla, **Phys. Rev. D**: **124004**, 2001; Bin Wang, Elcio Abdalla, R.B. Mann, **Phys. Rev. D**: **084006**, 2002.
- [12] Brady, P. and Smith, J. D., **Phys. Rev. Letters**, **75**, **7**, 1256, 1995.
- [13] Wang, B., Molina, C. and Abdalla, E., **Phys. Rev. D**, **63**, 084001, 2001.
- [14] Wang, B., Lin, C. and Abdalla, E., **Phys. Lett. B**, 2001.